Magnetism and Antiferroelectricity in MgB_6

Igor Popov, Nadjib Baadji, and Stefano Sanvito
School of Physics and CRANN, Trinity College, Dublin 2, Ireland
(Received 21 November 2011; published 8 March 2012)

We report on a density functional theory study demonstrating the coexistence of weak ferromagnetism and antiferroelectricity in boron-deficient MgB_6. A boron vacancy produces an almost one dimensional extended molecular orbital, which is responsible for the magnetic moment formation. Then, long-range magnetic order can emerge from the overlap of such orbitals above percolation threshold. Although there is a finite density of states at the Fermi level, the localized nature of the charge density causes an inefficient electron screening. We find that the Mg^{2+} ions can displace from the center of their cubic cage, thus generating electrical dipoles. In the ground state these order in an antiferroelectric configuration. If proved experimentally, this will be the first material without d or f electrons displaying the coexistence of magnetic and electric order.

DOI: 10.1103/PhysRevLett.108.107205 PACS numbers: 75.30.Hx, 71.55.−i, 75.10.Lp, 81.05.Zx

The discovery of weak ferromagnetism in La-doped CaB_6 by Young *et al.* [1] ignited a surge of research on alkaline-earth hexaborides, XB_6 (X = Ca, Sr, Ba) [2–8]. Initially the origin of the magnetism in these materials was attributed to possible transition-metal impurities [9]. However, subsequent experiments in high-purity CaB_6, SrB_6 and BaB_6 crystals [10–12] clearly indicated that the magnetism may be an *intrinsic* property of the XB_6 family, and not due to contaminations. Theoretical predictions for defective XB_6 assigned to boron vacancies, V_B, the primary cause of the magnetism. These introduce flat bands near the Fermi level, which spin-split due to the strong exchange interaction in the B p-shell [3,4,13,14]. Such predictions have been recently supported by experimental evidence [8,15,16], which also extends to CaB_6 and SrB_6 thin films [7].

In contrast to the heavy compounds of the XB_6 family, MgB_6 has received only little attention. This is mainly due to an early theoretical calculation, performed with empirical methods, suggesting the poor stability of MgB_6 compared to the more thermodynamically stable MgB_2, MgB_4, MgB_7 and MgB_{12} [17]. In addition the small Mg ionic radius, second only to Be among the alkalines, may result in a high ionic mobility and thus in Mg segregation. However, in contrast to this early prediction MgB_6 has been often observed experimentally [18], most notably with conclusive high resolution tunnelling electron microscopy [19]. In this letter we report on a density functional theory (DFT) study of the structural, electronic and magnetic properties of V_B-rich MgB_6. Our results point to a ferromagnetic ground state, which coexists with an antiferroelectric dipolar order. As such MgB_6 appears to be the first example displaying the coexistence of magnetic and electric order in a material not containing ions with partially occupied d or f shells.

Calculations are performed with the DFT numerical implementation contained in the SIESTA code [20]. The Perdew-Burke-Ernzerhof form of the generalized gradient approximation [21] is used for the structural optimization and for the calculation of the phonon dispersion. Additional calculations of the electronic properties use the Perdew-Zunger local density approximation (LDA) [22] including atomic self-interaction corrections (ASIC) [23]. The core electrons are described by norm-conserving pseudopotentials with partial core corrections [24], while the wave-function is expanded over a double-zeta numerical atomic orbital basis set including the following orbitals: Mg $3s$, Mg $3p$, B $2s$ and B $2p$. The charge density and the DFT potential are determined over a real-space grid with an equivalent mesh cutoff energy of 350 Ry, but a value of 700 Ry is used for calculating the phonon spectra. A 1728 k points dense mesh samples the Brillouin zone. Atomic relaxation is performed by conjugate gradient until the forces are smaller than 0.04 eV/Å (0.001 eV/Å for the phonon spectrum). Phonons are calculated by using the elementary unit cell; hence, only optical modes are considered.

We start our analysis by first looking at the defect-free crystal. XB_6 (X = Be, Mg, Ca) crystallizes in a halite cubic structure with the two inequivalent sites occupied, respectively, by the divalent X^{2+} ion and a B_6^{2-} octahedral cluster [see Fig. 1(a)]. The lattice parameter is determined by the size of the B_6 clusters and it is calculated to be 4.115 Å for MgB_6. The position of the cation however depends on the specific element. After structural relaxation Ca remains in the center-symmetric position, while Mg moves towards the face of the cubic cage and nests at 1.143 Å away from it. Interestingly, Be moves completely into the B_6 plane.

The potential energy surface of Mg^{2+} is plotted in Fig. 1(b) over one of the median planes cutting across the cubic cage, with the zero energy taken at the center-symmetric position. We observe four equivalent minima in the plane, which translate into six minima over the cubic

 © 2012 American Physical Society

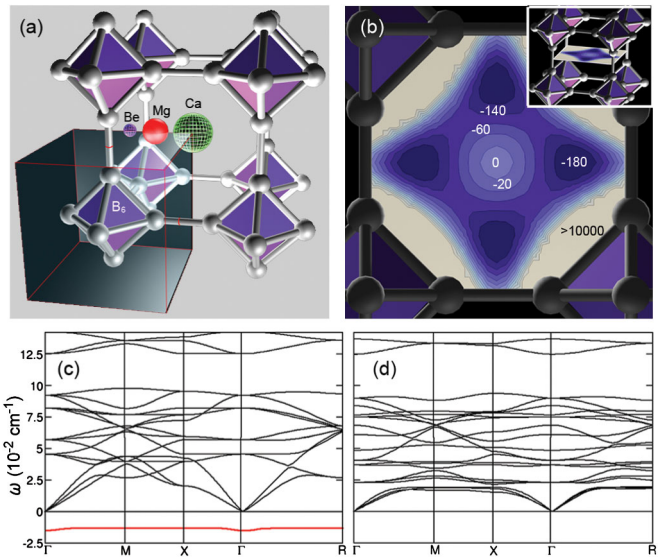

FIG. 1 (color online). MgB_6 structural properties. In (a) the XB_6 (X = Be, Mg, Ca) crystal structure, where the gray volume includes the unit cell. Note the different displacement of Ca, Mg, and Be within the B_6-defined cubic cage. (b) Potential energy surface (isovalues are in units of meV) for Mg^{2+} across the median plane of the cubic cage (shown in the inset). Phonon band structure for the center-symmetric MgB_6 crystal (c) and center-symmetric CaB_6 crystal (d).

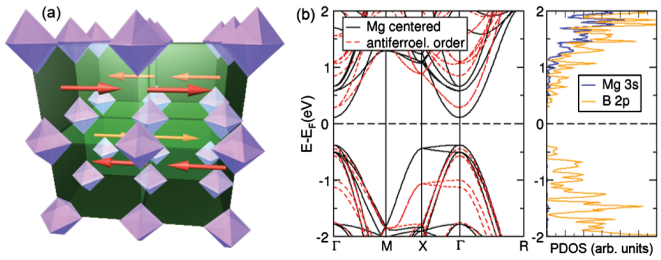

FIG. 2 (color online). Electronic structure of defect-free MgB_6. In (a) we present the type-C antiferroelectric order for a $3 \times 3 \times 3$ supercell. The arrows indicate the direction of the electric dipoles (atoms and bonds are removed for simplicity). In (b) a comparison of the electronic band structures for the center-symmetric and the type-C antiferroelectric ordered system obtained for $2 \times 2 \times 2$ supercell. The corresponding PDOS is presented in the rightmost panel.

volume. The potential barriers between the minima are around 70 meV, which indicate that the displaced Mg positions are stable at room temperature. Additional evidence of the Mg displacement is provided by the MgB_6 phonon spectrum [Fig. 1(c)] for the center-symmetric structure, which presents a triply-degenerate negative frequency mode. Note that the same is absent for the CaB_6 crystal [Fig. 1(d)], which remains undistorted.

Given the ionic character of MgB_6, the displacement of Mg^{2+} generates an electrical dipole parallel to the direction of the displacement. Standard (LDA) Berry-phase calculations give us an electrical polarization of 57.6 μC/cm^2 for an hypothetical ferroelectric phase. This however does not represent the correct long-range ferroic order. The overall dipolar arrangement is then computed by comparing total energy calculations for a $2 \times 2 \times 2$ supercell with different dipole configurations (ferroelectric, antiferroelectric of type A and type C and ferroelectric with only one dipole chain rotated) [25]. We find the energy minimum at the type-C antiferroelectric arrangement, which is illustrated in Fig. 2(a). Such a state is 226 meV lower than the ferroelectric one (per elementary unit cell), which suggests that it might be a relatively high-temperature phase.

The projected density of states (PDOS) of MgB_6 indicates that the material is semiconducting with a relatively small indirect (LDA) band gap of about 0.5 eV [see Fig. 2(b)]. This reduces to 0.27 eV if the calculation is performed at the GGA level. The conduction and valence bands have, respectively, Mg-s and B-p character, as expected from its ionic $Mg^{2+}(B_6)^{2-}$ nature. An ionic bonding favors the Mg^{2+} ion to move off-center in order to minimize the electrostatic energy. The same mechanism is ineffective for the heavier CaB_6 simply because of the much larger ionic radius of Ca^{2+}. Furthermore, as there is little covalent bonding between Mg and B_6 also the interaction between the dipoles has electrostatic nature and so an antiferroelectric order is expected [26]. Finally we note that the Mg displacement has little effect on the band structure as the antiferroelectric ground state remains insulating with an LDA gap of 0.73 eV [Fig. 2(b)].

Having characterized the electronic structure of defect-free MgB_6, we now move to discuss the effect of V_B in the crystal. The MgB_6 crystal bares symmorphic symmetry, so that its bands can be directly related to the energy levels of the B_6 cluster. The molecular states [Fig. 3(b)] are characterized according to the irreducible representations of the O_h group. The low lying T_{1u} state is of special interest. In fact a vacancy in B_6 crystal moves the T_{1u}-derived level upwards into the pristine gap of the crystal. T_{1u} is threefold degenerate with each of the levels in the manifold dominated by only one of B-p_i ($i = x, y, z$) orbitals. A vacancy also removes an electron so that B_5 is left with a single electron in nondegenerate orbital level. We then expect magnetic moment formation [27] with the spin-polarized charge density distributing along the direction where the B atom has been removed.

This qualitative picture is further confirmed with numerical DFT calculations. Since the self-interaction error in LDA usually precludes the correct description of defects in semiconductors, here we employ the ASIC scheme [23], which has been already proved successful in describing anion defects in the closely related MgO insulator [28]. In particular we perform calculations by using different values of the screening parameter α, ranging from $\alpha = 0$ (LDA) to $\alpha = 1$ (full ASIC), and compare spin-polarized (SP) and non-spin-polarized (NSP) results.

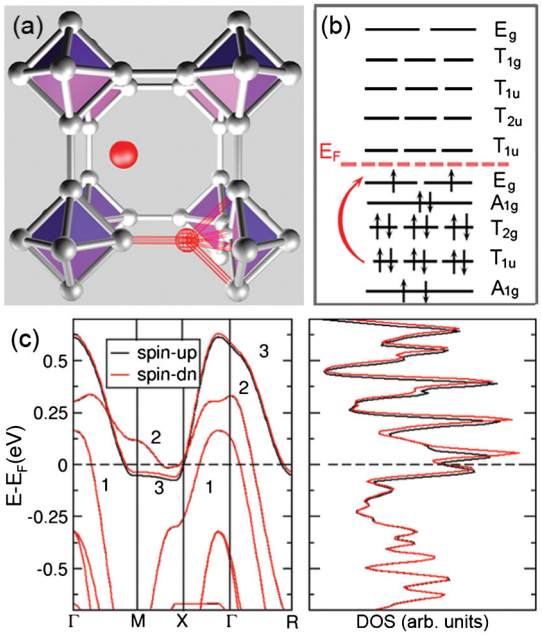

FIG. 3 (color online). Electronic structure of V_B-rich MgB_6. In (a) the geometry of a supercell containing one V_B. (b) shows the energy state diagram of a freestanding B_6 cluster. The red arrow indicates the rearrangement of states upon introduction of a vacancy in MgB_6 crystal. The electronic band-structure and DOS for the cell containing one vacancy are in panel (c).

Let us first discuss the magnetic moment formation associated to a single V_B in one $2 \times 2 \times 2$ supercell [see Fig. 3(a)]. LDA yields a cell magnetic moment of 3 mμ_B. Importantly, such a moment increases in the ASIC calculations. In fact, we find 414, 509, 565, and 617 mμ_B, respectively, for $\alpha = 0.25$, 0.5, 0.75, and 1. Also the total energy difference between the SP and the NSP solutions, $\Delta E(\alpha) = E_{SP} - E_{NSP}$, varies with the degree of ASIC considered (α). In particular, we find $\Delta E = 2$ meV for LDA and -23 meV, -44 meV, -116 meV, and -296 meV, respectively, for ASIC with $\alpha = 0.25$, 0.5, 0.75, and 1. As such we find that both the magnetic moment and its energy stability increase with increasing the amount of self-interaction corrections included. A value $\alpha = 0.5$ is usually considered appropriate for semiconductors so that we estimate a magnetic moment of around $1/2\mu_B$, with a formation energy well above the room temperature.

A deeper insight into the origin of the magnetic moment is obtained by looking at the band structure of the supercell containing one V_B [Fig. 3(c)]. As expected from the discussion about B_6 now the system has a metallic electronic structure with three bands crossing the Fermi level, E_F [labeled with 1, 2, and 3 in Fig. 3(c)]. Their dispersion is typical of a semimetal with both electron (from M to X and at R) and hole (at Γ) pockets at the E_F. As the three bands are non-orbital-degenerate the system is not prone to the Jahn-Teller distortion, which might compete with the formation of the moment. Importantly only the electron carrying band [3 in Fig. 3(c)] spin-splits, while the other two remain non-spin-polarized. Recalling the fact that the Stoner exchange parameter is rather large in the $2p$ shell [14], the spin-splitting occurs in bands with a narrow bandwidth, i.e., in bands that can provide a large DOS at E_F. This is the case of the electron carrying band (3), which has a bandwidth of 0.68 eV to be compared with 1.3 and 1.2 eV for the other two. Such a picture of magnetic moment formation due to narrow bands is robust with both the number and the position of the vacancies as we tested for a $2 \times 2 \times 2$ supercell with two V_B's at different positions.

The unique directional nature of the V_B-derived electronic bands at E_F is provided in Fig. 4(a), where we show the local density of states (LDOS), obtained within the energy range ($E_F - 0.05$ eV, $E_F + 0.05$ eV). From the figure it emerges that the electron cloud is delocalized only along the direction defined by the center of vacant B_5 cluster and by the position of V_B, as expected from the T_{1u} symmetry. The contribution to the DOS from the B atoms which do not lie along such a preferential direction is negligible [Fig. 4(b)]. The presence of multiple V_B's does not alter this picture. Figure 4(c) shows the LDOS of two V_B's at different positions, with formation of two directional states oriented in different directions and not overlapping among each other.

The formation of a moment is not a sufficient condition for long-range magnetism [28]. The picture emerging from our electronic structure calculations is that of magnetic moments associated to directional extended molecular orbitals at the B_5 clusters. We then expect magnetism

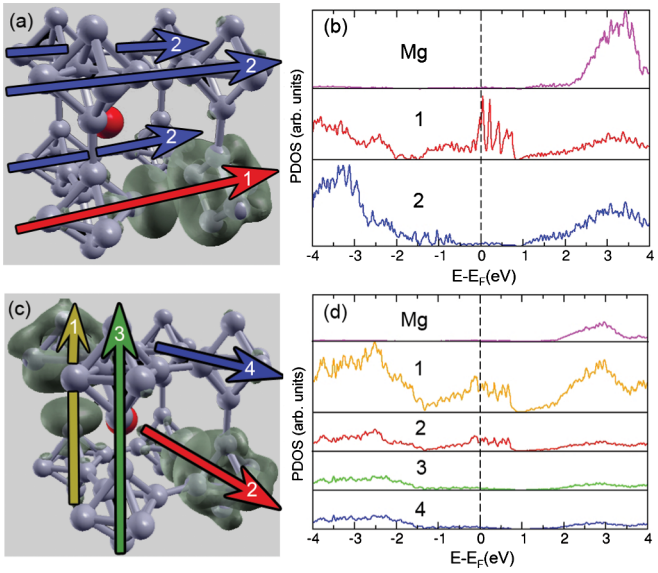

FIG. 4 (color online). Local density of states around the Fermi level of a MgB_6 crystal with one (a) and two (c) vacancies per $2 \times 2 \times 2$ supercell. In the panels (b) and (d) we show the DOS projected over different subsets of B atoms. In particular we project over B atoms along the directions indicated by the arrows in the panels (a) and (c).

only when the magnetic-moment-carrying levels of different B_5 clusters overlap. We have checked that distant V_B's are magnetically coupled by calculating the total energy difference between a ferromagnetic and an antiferromagnetic configuration of a $4 \times 2 \times 2$ supercell. We find that, when the two B_5 clusters are 8.23 Å apart, there is an energy difference of 32 meV/vacancy ($\alpha = 0.5$) in favor of the ferromagnetic solution. Although more calculations are needed at other V_B concentrations and for different V_B-V_B separations, we may yet conclude that our calculations point to both the moment formation and exchange coupling between distant moments. A long-range order is then expected when, typically randomly distributed, the magnetic moments form a percolation network. Two important considerations must be made here. First, as one missing B over the B_6 cluster is responsible for the moment and percolation is between the B_6 clusters, a cluster percolation threshold of x is achieved by removing only $x/6$ B ions. Second, we remark that the magnetism is related to the B_6 sublattice only, so that our results should be transferable to other XB_6 materials. However, we expect that the local electrical dipole associated to the Mg^{2+} ions in cages bordered by B_5 clusters, will be different in direction and magnitude from that of the vacancy-free case.

Finally we wish to spend a few words on the possibility of the coexistence of both the ferromagnetic and antiferroelectric order. In general a ferroic state cannot be sustained in a metal because of the screening from the free electrons. The situation here is however more complex as, although there is density of states at the Fermi level, this is associated to partially localized states. Their screening can be inefficient to a point that local electric dipoles still form [29,30]. Our results indeed confirm such a hypothesis as the Mg ions remain in their off-center positions as B vacancies are introduced in the cell. Notably, the strong directional nature of the charge density at the Fermi level suggests that such an inefficient screening persists locally even above the percolation threshold.

In conclusion, we have investigated structural, electronic and magnetic properties of ideal and defective $MgB_{6-\delta}$ crystals. These present the coexistence of weak magnetism and potentially antiferroelectricity. The local magnetic moments originate from a V_B-related impurity band and the dipole moments from the displacement of the Mg^{2+} ions within the cubic cage. Long-range magnetism can be sustained only above the magnetic percolation threshold and the antiferroelectric state can coexist with a finite DOS at the Fermi level because of the incomplete screening from the localized charge. If proved experimentally, this will be the first example of coexistence of magnetic and electric order in a material not incorporating ions with partially occupied d or f shells.

This work is sponsored by Science Foundation of Ireland (SFI) under the CSET grant underpinning CRANN. N. B. acknowledges support from SFI (grant No. 08/ERA/I1759). Computational resources have been provided by the HEA IITAC project managed by TCHPC.

[1] D. P. Young *et al.*, Nature (London) **397**, 412 (1999).
[2] H. J. Tromp, P. van Gelderen, P. J. Kelly, G. Brocks, and P. A. Bobbert, Phys. Rev. Lett. **87**, 016401 (2001).
[3] R. Monnier and B. Delley, Phys. Rev. Lett. **87**, 157204 (2001).
[4] D. M. Edwards and M. I. Katsnelson, J. Phys. Condens. Matter **18**, 7209 (2006).
[5] B. Lee and L.-W. Wang, Appl. Phys. Lett. **87**, 262509 (2005).
[6] S. Okatov, A. Ivanovskii, Y. Medvedeva, and N. Medvedeva, Phys. Status Solidi B **225**, R3 (2001).
[7] L. S. Dorneles, M. Venkatesan, M. Moliner, J. G. Lunney, and J. M. D. Coey, Appl. Phys. Lett. **85**, 6377 (2004).
[8] B. K. Cho *et al.*, Phys. Rev. B **69**, 113202 (2004).
[9] K. Matsubayashi, M. Maki, T. Tsuzuki, T. Nishioka, and N. K. Sato, Nature (London) **420**, 143 (2002).
[10] P. Vonlanthen *et al.*, Phys. Rev. B **62**, 10076 (2000).
[11] H. R. Ott *et al.*, Physica (Amsterdam) **281–282B**, 423 (2000).
[12] S. E. Lofland, B. Seaman, K. V. Ramanujachary, N. Hur, and S. W. Cheong, Phys. Rev. B **67**, 020410(R) (2003).
[13] J. X. Cao, Y. Zhu, Z. Q. Yang, and R. Q. Wu, Phys. Rev. B **79**, 132404 (2009).
[14] J. F. Janak, Phys. Rev. B **16**, 255 (1977).
[15] K. Maiti, V. R. R. Medicherla, S. Patil, and R. S. Singh, Phys. Rev. Lett. **99**, 266401 (2007).
[16] K. Maiti, Europhys. Lett. **82**, 67006 (2008).
[17] G. Moseev and A. Ivanovskii, Inorg. Mater. (USSR) **41**, 1061 (2005).
[18] S. Chen, M. Majoros, J. MacManus-Driscoll, and B. Glowacki, Physica (Amsterdam) **418C**, 99 (2005); S. Lee *et al.*, J. Phys. Soc. Jpn. **70**, 2255 (2001); R. Wagner, R. Kampmann, and P. W. Voorhees, *Phase Transformation in Materials*, edited by G. Kostorz (Wiley-VCH, Winheim, 2001), p. 309; T. B. Massalski, H. Okamoto, P. R. Subramanian, and L. Kacprzak, *Binary Alloy Phase Diagrams* (ASM International, Materials Park, Ohio, 1990), p. 498.
[19] S. Li *et al.*, Appl. Phys. Lett. **81**, 874 (2002).
[20] J. M. Soler *et al.*, J. Phys. Condens. Matter **14**, 2745 (2002).
[21] J. P. Perdew, K. Burke, and M. Ernzerhof, Phys. Rev. Lett. **77**, 3865 (1996).
[22] J. P. Perdew and A. Zunger, Phys. Rev. B **23**, 5048 (1981).
[23] C. Das Pemmaraju, T. Archer, D. Sánchez-Portal, and S. Sanvito, Phys. Rev. B **75**, 045101 (2007).
[24] N. Troullier and J. L. Martins, Phys. Rev. B **43**, 1993 (1991).
[25] E. O. Wollan and W. C. Koehler, Phys. Rev. **100**, 545 (1955).
[26] N. A. Hill, J. Phys. Chem. B **104**, 6694 (2000).
[27] C. D. Pemmaraju and S. Sanvito, Phys. Rev. Lett. **94**, 217205 (2005).
[28] A. Droghetti, C. Pemmaraju, and S. Sanvito, Phys. Rev. B **81**, 092403 (2010).
[29] P. W. Anderson and E. I. Blount, Phys. Rev. Lett. **14**, 217 (1965).
[30] J. I. Gersten and M. Weger, Phys. Rev. B **65**, 214530 (2002).